# Reactions Between Liquid CaO-$SiO_2$ Slags and Graphite Substrates

JESSE F. WHITE, JAEWOO LEE, OSCAR HESSLING, and BJOERN GLASER

In this study, the spreading and infiltration behavior of liquid slag in contact with different grades of graphite was investigated. The wetting and infiltration of slag into graphite were found to be highly material dependent. The reduction of silica by carbon is a characteristic of the system, and it generates gaseous products as evidenced by the observation of bubble formation. The higher the temperature and silica activity of the slag is, the greater the slag infiltration and the faster the rate of spreading. Silicon infiltrated into the graphite substrates much deeper than the oxide phases, indicating gas-phase transport of SiO(g) into the graphite pores. Fundamentally, in this system where the liquid and substrate are reacting, the driving force for spreading is the movement of the system toward a lower total Gibbs energy. Reduction of silica in the slag near the interface may eventually lead to the formation of a solid, CaO-rich layer, slowing down or stopping the reduction reaction.

DOI: 10.1007/s11663-016-0788-5


## I. INTRODUCTION

GRAPHITE is an exceptional refractory material that is used extensively in the smelting, melting, refining, and crystallization of silicon as well as in other metallurgical systems where carbon solubility is limited. Besides unsurpassed refractoriness, at low oxygen potential, graphite is chemically stable and has high resistance to thermal shock. Graphite also has the added benefit of being a soft material that is easily machinable to almost any shape or form. In actuality, commercially available synthetic graphites are not simple materials—there are a panoply of graphite grades on the market from numerous suppliers, and the manufacturing processes and production recipes can be quite diverse. As such, the thermophysical properties as well as the chemical reactivity of these different graphite grades can widely vary.

Several published studies investigated the wetting of carbonaceous substrates with slags; all of these studies employed high-temperature sessile drop apparatuses to measure the change in apparent contact angle of a molten slag droplet on a substrate over time, with several employing scanning electron microscopy (SEM) to analyze the reaction interfaces.[1–10] Most studies were in the context of ironmaking processes, and thus, they involved iron-bearing slags reacting and spreading on coal char, coke, and both natural and synthetic graphite substrates.[1–8] The reduction reaction of FeO by the carbon substrate has been found to play a major role in the wetting behavior in such systems.[3,4]

Some studies focused specifically on the wetting behavior of nonferrous slags: Recently, Oh and Lee measured the wetting of CaO-$SiO_2$-$Al_2O_3$-MgO slags on pressed coke substrates at 1773 K (1500 °C); they attributed the process of slag wetting to the formation of SiC at the slag–graphite interface.[9] Heo, Lee, and Chung made similar measurements of the wetting of CaO-$SiO_2$(-$Al_2O_3$) slags on MgO-C and graphite substrates at 1873 K (1600 °C).[10]

Some studies made careful analyses of the kinetics of slag–graphite reactions, including measurements of the concentration of CO and $CO_2$ gas in the furnace off-gas using a mass spectrometer, and the change in slag composition with time.[4,7,8]

Liquid slags react with carbon in surprisingly complex ways. The reduction of silica in the slag and the adverse effect of increasing slag basicity (decreasing silica activity) on the spreading of slag has been documented in several of these studies.[1,5,7–9] Gas evolution during wetting of carbonaceous substrates with slag has also been described by several others.[1,3,4,8]

Some industrial processes contain both a liquid metallic phase and a slag phase in contact with a graphite refractory, such as during slag refining of silicon. In slag refining of metals, proper wetting of graphite by liquid slag could prove to have a beneficial impact: The lifespan of graphite refractories could be prolonged by reacting with slag to protect the refractory from infiltration and reaction with the metallic phase.

The objective of the current study was to explore further the melting behavior of liquid slag in contact with different synthetic graphite grades from a fundamental perspective to understand better the reactions involved, and to determine to what extent this phenomenon can be fully exploited.

JESSE F. WHITE, Research Scientist, JAEWOO LEE, Postdoctoral Research Associate, OSCAR HESSLING, Graduate Student, and BJOERN GLASER, Assistant Professor, are with the Department of Materials Science and Engineering, KTH Royal Institute of Technology, SE-100 44 Stockholm, Sweden. Contact e-mail: jfwhite@kth.se

Manuscript submitted June 23, 2016.
Article published online September 26, 2016.

## II. EXPERIMENTAL

A high-temperature sessile drop system was used in this investigation, which is illustrated in Figure 1. The experimental technique was very similar to a previous study[11] that investigated the wetting of graphite by liquid silicon; the system is also described in a previous publication.[12] A horizontal Entech electrical tube furnace with Kanthal Super heating elements and an alumina reaction tube (70 mm inner diameter) was used in this study. On one end of the tube, an internally water-cooled quenching chamber sealed the tube with a viton o-ring; the opposite end of the tube was sealed in a similar fashion with a water-cooled aluminum cap with a sealed quartz glass window. The specimen was placed on a graphite carriage that transported the specimen in and out of the hot zone of the furnace. A water-cooled pushrod, sealed with a shaft packing, was connected to the graphite carriage, which in turn was fastened to a screw drive that enabled the precise positioning and movement of the specimen to reproducibly control heating and cooling rates.

A Eurotherm controller was used to set and maintain the target furnace temperature, with an even temperature zone was defined as ±2 K from the target temperature. A control thermocouple was a Type B (Pt-6 pct Rh/Pt-30 pct Rh) thermocouple (mounted on the wall of the furnace), which was positioned in the hot zone of the furnace outside of the reaction tube. A measurement thermocouple was a Type C (W/W-5 pct Re), 1 pct accuracy, and was mounted axially in the pushrod and carriage, with the tip inside the carriage body positioned directly under the substrate.

High-purity argon gas was metered using a Bronkhorst mass flow meter (±0.5 pct accuracy). The reaction gas entered on the window end, passed through the tube, and exited out of the quenching chamber.

A Leica V-LUX3 digital camera with full HD video (1920 × 1080) capability at 30 fps was mounted with a view into the quartz glass window on the end of the furnace opposite the quenching chamber. Video recording was initiated when the specimen began to melt.

### A. *Materials Preparation*

Two binary CaO-$SiO_2$ master slags were prepared prior to the experiments by fusing high-purity fused silica and calcium oxide, which in turn was prepared by calcining precipitated calcium hydroxide, in a graphite crucible and subsequently granulated in water. A wide interval in the compositions of the slags was chosen to examine the effect of silica activity on the wetting behavior. As seen in Figure 2, which is a binary phase diagram for the CaO-$SiO_2$ system, at 46 mass pct $SiO_2$, the composition was close to the first eutectic composition. The second slag was the second eutectic composition with a higher silica content of 63 mass pct. Table I summarizes the properties of the slags used in this study.

Graphite qualities were chosen based on industrial relevance. Substrate disks were milled out of three different grades of graphite, and as can be seen in Table II and Figure 3, there is large disparity in the physical characteristics of these graphite grades.

The substrates were 38 mm in diameter and 8 mm thick. Prior to the runs, the disks were heated at 393 K (120 °C) for at least 2 hours to remove any adsorbed water on the surfaces.

### B. *Experimental Procedure*

In preparation for each experiment, 2.5 g of granulated slag was pressed into a 10-mm-diameter pellet. The graphite substrate was cleaned with ethanol and after drying placed on the carriage. The slag pellet was positioned on top of the graphite substrate, and the system was sealed with the carriage positioned in the quenching chamber. The reaction tube was evacuated with a vacuum pump for 30 minutes and back-filled with argon. To commence the run, the flow of reaction gas started at 0.05 L/min, while the furnace control sequence was initiated to ramp the temperature up to 1823 K or 1873 K (1550 °C or 1600 °C) at 2 degrees per minute. Video recording with the digital camera was started as soon as the melting temperature of the slag was exceeded. After 30 minutes of video recording, the rest of the experiment was photographed at 5-minute intervals.

At the end of each run, the carriage was rapidly extracted from the furnace into the water-cooled quenching chamber by activating the mechanical screw drive. In most of these runs, there was sufficient time for the slag to completely spread on the graphite substrate; however, some experiments were stopped when slag reached the edge of the graphite substrate. After quenching, the specimens were taken out of the furnace and prepared for scanning electron microscopy (SEM) analysis and electron-dispersive spectroscopy (EDS) using a Hitachi S-3700N coupled with a Bruker XFlash Detector 4010. Still images were extracted from the video files, and from these, the rate of spreading of slag (apparent contact angle) on the graphite substrate was quantified.

## III. RESULTS

Table III outlines the conditions of the experiments that were conducted and the duration of each experiment. The changes in apparent contact angle as a function of time for the two slag compositions on each graphite substrate were recorded, and the results are presented in Figures 6 through 9.

### A. *Wetting*

Figure 4 is composed of snapshots taken at time intervals during Run no. SG11, showing the spreading of Graphite B by Slag 1 at 1823 K (1550 °C). The slag pellet fused and formed a droplet on the graphite substrate as seen in Figure 4(a) designated as $t = 0$. As molten slag was drawn into the pores by capillary action, the height of the droplet and apparent contact angle decreased dramatically (by 20 minutes), as shown in Figure 4(b). After this initial infiltration, the apparent contact angle decreased slightly until bubble formation started occurring, as shown in Figure 4(c). Eventually,

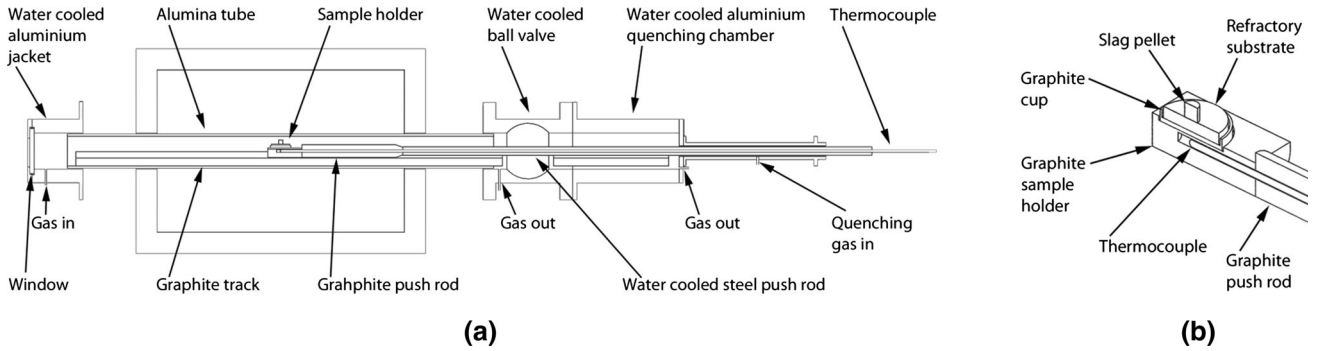


Fig. 1—Schematic of experimental apparatus showing the constituent parts. (*a*) System schematic and (*b*) sample holder details. Adapted from Ref. [12].

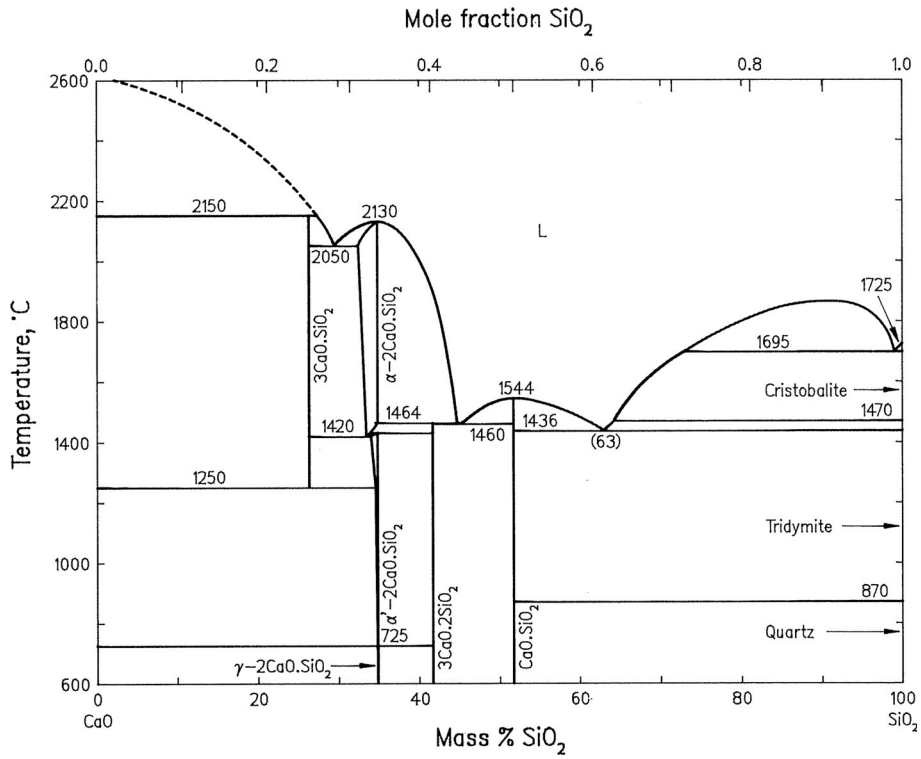


Fig. 2—Phase diagram for the binary CaO-$SiO_2$ system.[13]

**Table I. Compositions and Properties of the Slags**

| | Comp. (mass pct) | | $a_{SiO_2(s)}$* | | | Viscosity (Pa s)* | |
|---|---|---|---|---|---|---|---|
| Slag No. | $SiO_2$ | CaO | 1823 K (1550 °C) | 1873 K (1600 °C) | Liquidus Temp. [K (°C)]* | 1823 K (1550 °C) | 1873 K (1600 °C) |
| 1 | 46 | 54 | 0.16 | 0.15 | 1770 (1497) | 0.18 | 0.14 |
| 2 | 63 | 37 | 0.84 | 0.78 | 1712 (1439) | 1.25 | 0.92 |

*Calculated with Factsage.[14]

bubble formation attenuated and the droplet continued spreading, reaching a maximum by 140 minutes.

Images of gas bubble formation on top of the slag droplets observed in various experiments are seen in Figure 5. Bubble formation was observed in all but the tests with Slag 1 on the Graphite C substrate.

Figure 6 plots the apparent contact angle of Slag 1 on the graphite substrates with time at 1823 K (1550 °C). The spreading behavior was seen to be quite different for each graphite substrate: Although the initial rate of spreading was similar for all three types, the equilibrium contact angles and times to reach a stable contact angle

Table II. Characteristics of the Graphite Substrates[12]

| Graphite Grade | Manufacturing Method | Ash Content (mass pct) | Bulk Density (g/cm$^3$) | C.T.E. $\parallel/\perp$ ($10^{-6}$/K) | Max. Grain Size (mm) | Open Porosity (pct) |
|---|---|---|---|---|---|---|
| A | isostatic | 0.03 | 1.77 | 4.3 | 0.015 | 9 |
| B | vibration-molded | 0.07 | 1.73 | 1.2/1.9 | 0.8 | 15 |
| C | extruded | 0.08 | 1.72 | 3.0/3.5 | 0.8 | 16 |

varied considerably. Spreading on Graphite A (the isostatic quality with lowest open porosity) took about 20 minutes to reach a stable apparent contact angle of about 100 deg. For Graphite B (vibration molded quality), spreading occurred to a considerably lower apparent contact angle of about 40 deg after a long period of time (90 minutes) Interestingly, slag wetting on Graphite C, which is an extruded graphite quality with the highest open porosity, reached the highest stable apparent contact angle of about 130 deg in a relatively short period of time (20 minutes).

At the higher temperature of 1873 K (1600 °C), the spreading of Slag 1 was more rapid. Figure 7 shows that at this higher temperature, slag on Graphite A attained a much lower contact angle of slightly over 40 deg by about 80 minutes; in this case, the experiment was stopped due to the slag reaching the edge of the substrate, and it does not appear that a stable contact angle was reached. Slag spreading on Graphite B was also more rapid, reaching 60 deg just after 20 minutes (this experiment was also stopped when slag reached the substrate edge). Spreading of slag on Graphite C was considerably different at the higher temperature where a much lower contact angle of around 40 deg was attained after 230 minutes.

Increased silica content in the slag profoundly influences the spreading behavior. Figure 8 shows the wetting of Slag 2 on the graphite grades at 1823 K (1550 °C). It is immediately apparent that the final contact angles were considerably lower on all graphite grades than for the slag with lower silica content at the same temperature (compared with Figure 6). The rate of spreading on Graphites A and C are similar, although in this case, the apparent contact angle on Graphite C was lower. Also apparent is the marked change in spreading rate on Graphite B, where after only 20 minutes, the contact angle reached 30 deg (compared with 130 minutes to reach nearly the same angle for the Slag 1 as seen in Figure 6). Stable contact angles are not reached on any substrate.

Lastly, Figure 9 shows the combined effect of increased silica content and higher temperature on the spreading rate. For all graphite grades, Slag 2 had markedly higher rates of spreading with a 50-deg increase in temperature. Spreading on Graphites A and B changed very rapidly. Slag wetting on Graphite C attained 40 deg by 90 minutes, which is considerably faster than at the lower temperature (compared with Figure 8).

The viscosity of the slag does not seem to impact the rate of spreading: From Table I, it can be seen that the viscosity of Slag 2 is nearly an order of magnitude greater than Slag 1, and the increase in temperature from 1823 K to 1873 K (1550 °C to 1600 °C) does not significantly decrease the slag viscosities.

### B. *Infiltration*

As seen in Figure 2, the internal structures of the different graphite grades are significantly different. The isostatically pressed graphite quality Graphite A has by far the finest and most homogeneous internal structure, exhibiting small, evenly sized, and spaced pores. This is in contrast to Graphite B, which is a vibration-molded quality that has large, irregularly shaped pores of widely varying size and distribution. Graphite C, the extruded quality, has the highest open porosity (see Table I), and yet, it has smaller and more evenly distributed pores compared with Graphite B.

To examine the extent of infiltration, scanning electron microscopy (SEM) and electron-dispersive spectroscopy (EDS) mapping were conducted for the elements oxygen, calcium, and silicon. It should first be noted that it does not appear that any $SiO_2$ and CaO present as ash constituents can be detected in the EDS elemental mapping; therefore, the presence of Si and Ca as shown in the mapping is solely attributed to the infiltration of slag.

Figures 10 through 12 show Slag 1 infiltration into the graphite substrates. From the SEM micrograph for Graphite A shown in Figure 10(a), it is evident that liquid slag infiltrates the pores in the Graphite A substrate nearest the slag–graphite interface. Figures 10(b) and (c) show that oxygen, calcium, and silicon are spatially associated, which is expected since it is a binary calcium silicate slag. Nevertheless, comparison of Figures 10(b) through (d) reveal that silicon infiltrates somewhat deeper into the pores of the substrate than either oxygen or calcium. In Figure 11(a), some of the large pores in Graphite B nearest the interface are not filled with slag. In Figures 11(b) through (d), it can be seen that oxygen, calcium, and silicon are clearly associated. For Graphite C, shown in Figure 12(a), many visible pores have not been infiltrated by slag. EDS mapping in Figures 12(b) through (d) again reveals that O, Ca, and Si are associated, but even more pronounced than for Graphite A, and silicon infiltrates deepest into the graphite substrate. The depth

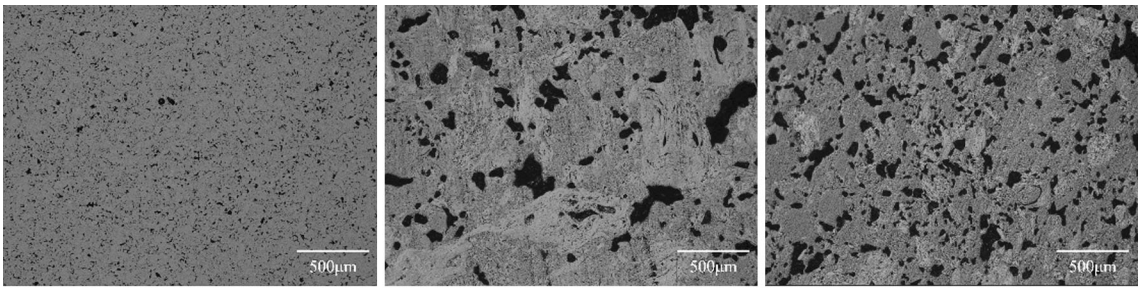


Fig. 3—Optical micrographs of surfaces of graphite substrates at 50 times magnification. (*a*) Graphite A, (*b*) Graphite B, and (*c*) Graphite C. Reprinted from Ref. [12].

**Table III. Experimental Conditions[12]**

| Run No. | Slag No. | Graphite Substrate | Temperature [K (°C)] | Duration (min) |
|---|---|---|---|---|
| SG13 | 1 | A | 1823 (1550) | 150 |
| SG2 | 1 | A | 1873 (1600) | 120 |
| SG11 | 1 | B | 1823 (1550) | 140 |
| SG1 | 1 | B | 1873 (1600) | 150 |
| SG7 | 1 | C | 1823 (1550) | 120 |
| SG8 | 1 | C | 1873 (1600) | 60 |
| SG15 | 1 | C | 1873 (1600) | 210 |
| SG17 | 2 | A | 1823 (1550) | 160 |
| SG14 | 2 | A | 1873 (1600) | 60 |
| SG12 | 2 | B | 1823 (1550) | 25 |
| SG16 | 2 | B | 1873 (1600) | 60 |
| SG19 | 2 | C | 1823 (1550) | 210 |
| SG18 | 2 | C | 1873 (1600) | 60 |

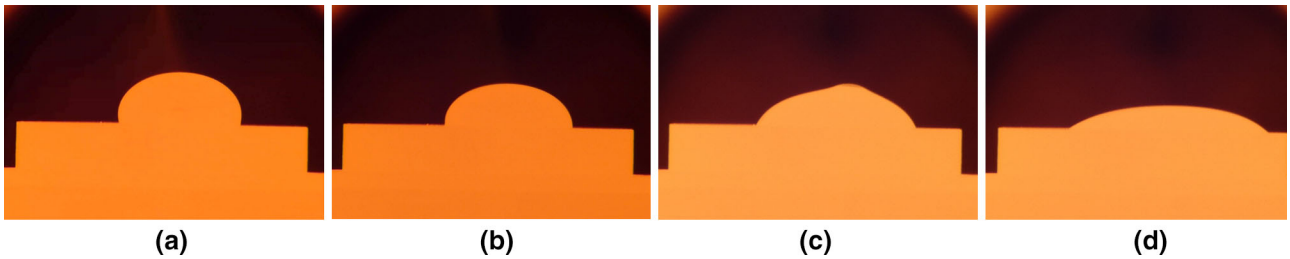


Fig. 4—Spreading of Slag 1 on Graphite B at 1823 K (1550 °C). (*a*) $t = 0$ min, (*b*) $t = 20$ min, (*c*) $t = 103$ min, and (*d*) $t = 140$ min. Reprinted from Ref. [12].

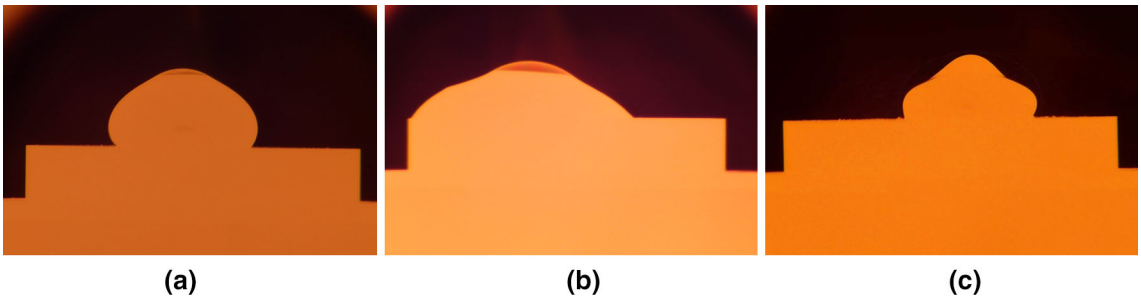


Fig. 5—Instances of bubble formation on the surfaces of the slag droplets. (*a*) Slag 1 on Graphite A, 1823 K (1550 °C), (*b*) Slag 1 on Graphite B, 1873 K (1600 °C), and (*c*) Slag 1 on Graphite A, 1873 K (1600 °C).

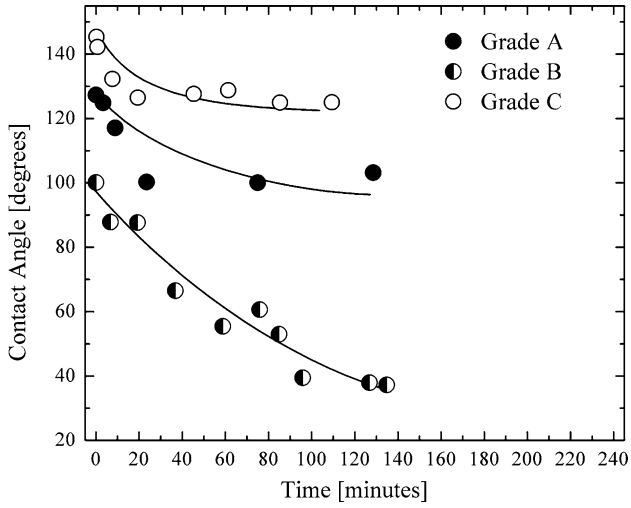


Fig. 6—Apparent contact angle as a function of time of Slag 1 on the different graphite grades at 1823 K (1550 °C).

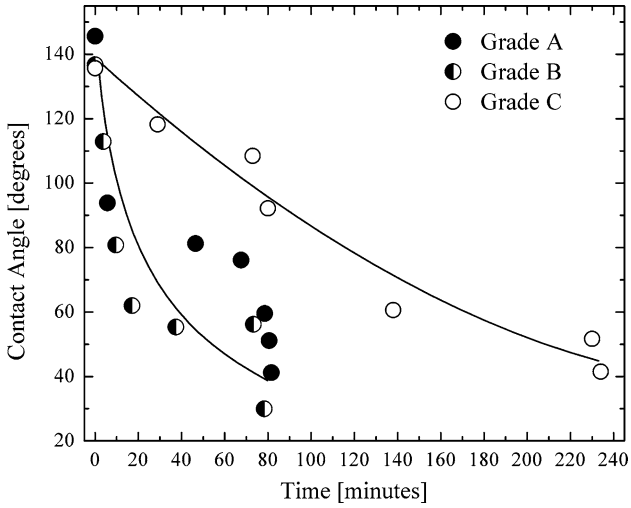


Fig. 7—Apparent contact angle as a function of time of Slag 1 on the different graphite grades at 1873 K (1600 °C). Adapted from Ref. [12].

of infiltration is the least in Graphite A and the greatest in Graphite B.

Figures 13 and 14 show infiltration of Slag 2 at 1873 K (1600 °C) into Graphites A and B, respectively. Again, a clear association of O, Ca, and Si is observed in Figures 13(b) through (d), but as seen in (d), deeper infiltration of silicon compared with O or Ca is observed. The SEM micrograph in Figure 14(a), which is at lower magnification than Figure 11, shows that slag has penetrated into striated pores or micro-cracks at the interface. Many unfilled pores are evident. Once again, silicon has infiltrated to a greater extent than either oxygen or calcium (CaO) as seen in Figures 14(b) through (d).

## IV. DISCUSSION

It is evident from the present results that the wetting and infiltration in this case are not simple mechanical

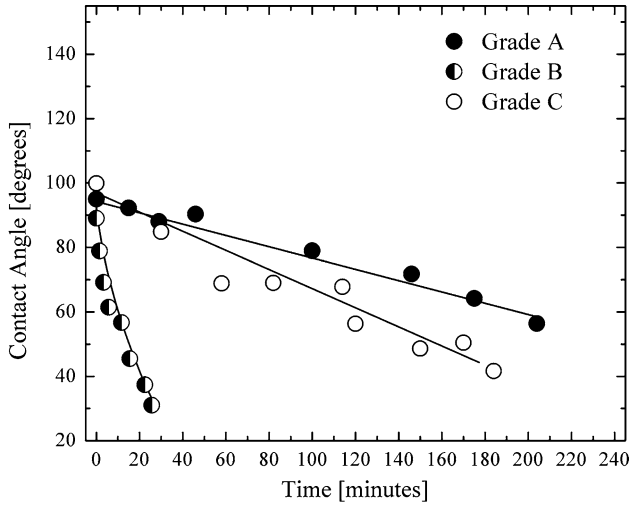


Fig. 8—Apparent contact angle as a function of time of Slag 2 on the different graphite grades at 1823 K (1550 °C).

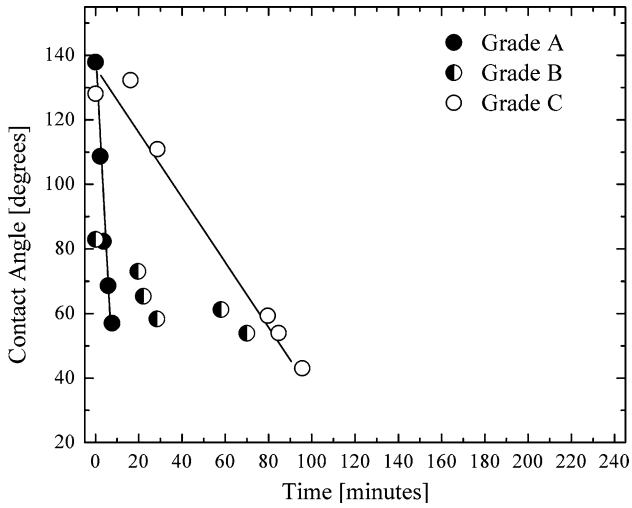


Fig. 9—Apparent contact angle as a function of time of Slag 2 on the different graphite grades at 1873 K (1600 °C). Adapted from Ref. [12].

phenomena. Chemical reactions between the slag components and the substrate occur, and the characteristics of these reactions seem to play a role in the wetting and infiltration behavior.

### A. *Interfacial Chemical Reactions*

The Si-C-O system is quite complex with many possible reaction paths, and there are many publications that support this; most of these deal with the reduction of pure solid-state silica by carbon.[15–19] The reaction:

$$SiO_2(s,l) + 2C(gr) = Si(l) + 2CO(g),$$

is not a valid equilibrium reaction for the reason that Si and C cannot coexist in thermodynamic equilibrium due to the formation of SiC. The common consensus is that silica is first reduced to silicon monoxide vapor:[7,16–19]

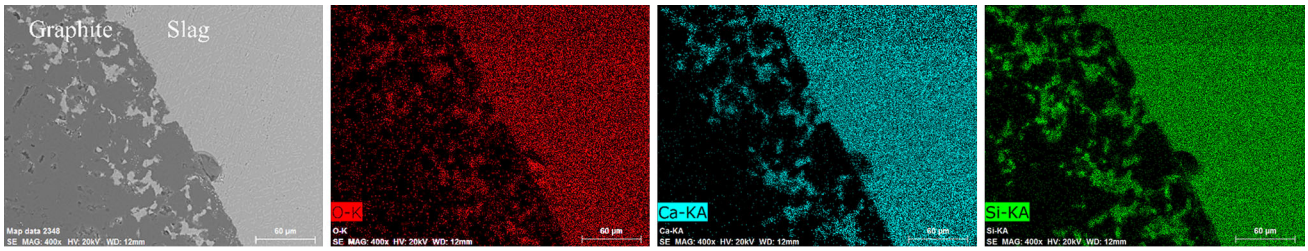


Fig. 10—SEM micrograph and EDS mapping showing extent of infiltration of Slag 1 into Graphite A at 1873 K (1600 °C) after 120 min (Run SG2). (*a*) SEM micrograph, (*b*) depth of O infiltration, (*c*) depth of Ca infiltration, and (*d*) depth of Si infiltration.

$$SiO_2(s,l) + C(gr) = SiO(g) + CO(g). \quad [1]$$

Fundamentally, this reaction can be written as:

$$SiO_2(s,l) = SiO(g) + \frac{1}{2}O_2(g), \quad [2]$$

With the oxygen potential controlled by the reaction:

$$C(gr) + \frac{1}{2}O_2(g) = CO(g). \quad [3]$$

The exact reaction mechanism for silica reduction can be debated and is worthy of further study.

Silicon carbide readily forms under these conditions as well. Silicon monoxide vapor and carbon will subsequently react to form silicon carbide according to:

$$SiO(g) + 2C(gr) = SiC(s) + CO(g). \quad [4]$$

The overall reaction path to form silicon carbide is considered to be a combination of Eqs. [1] and [2].[16–19]

Gas bubble formation on the slag droplet as revealed in Figures 4 and 5 is taken as evidence that Eq. [1] is proceeding and generating SiO(g) and CO(g). Chemical equilibrium is not attained in the time frame of these experiments—given enough time, the slag would have continued to react with the graphite to form SiO(g) and be transported away from the reaction interface in such an open system, leading to a continual reduction of the silica activity in the slag. Incidentally, this would also limit the extent of Eq. [4] at the slag–graphite interface. It is notable that the presence of a distinct SiC phase at the slag–graphite interface is not observable in any SEM micrograph; this is in contrast to during the study of slag wetting of cokes.[9] Neither was any silicon phase found present.

It is speculated that at the slag–carbon interface, bubbles of gaseous product form by heterogeneous nucleation at irregularities or pores on the substrate surface. Likely, bubbles of many different sizes are continually being formed at the interface. After reaching a certain size where the buoyancy force overcomes the surface tension force, a bubble detaches and rises through the liquid slag phase.

As the activity of silica in the slag decreases with time due to SiO(g) evolution and subsequent escape from the system, the driving force for this reaction should likewise decrease, and below a certain silica activity threshold, the reaction will cease. A simple thermodynamic analysis of Eq. [1] is as follows. The Gibbs energy of this reaction can be calculated from the relationship:

$$\Delta G_{[1]} = \Delta G^{\circ}_{[1]} + RT \ln Q, \quad [5]$$

where $Q$ is the reaction quotient:

$$Q_{[1]} = \frac{p_{SiO(g)} \cdot p_{CO(g)}}{a_{SiO_2(s)} \cdot a_{C(gr)}}. \quad [6]$$

The total gas pressure of the reaction is approximated to be $P_T = p_{SiO(g)} + p_{CO(g)} = 1$ atm, so that $p_{SiO(g)} = p_{CO(g)} = 0.5$ atm. The activity of carbon is taken as unity. Calculations of the activities of silica, with reference to pure solid cristobalite, are listed in Table I. For Eq. [1], the standard state Gibbs energies were calculated using Factsage:[14]

$$\Delta G^{\circ}_{[1],1823\,K\,(1550\,^{\circ}C)} = 2122\ J/mol \quad [7]$$

$$\Delta G^{\circ}_{[1],1873\,K\,(1600\,^{\circ}C)} = -18,644\ J/mol, \quad [8a]$$

$$\Delta H^{\circ}_{[1],1873\,K\,(1600\,^{\circ}C)} = 760,448\ J/mol, \quad [8b]$$

Figure 15 is a plot of the Gibbs energy of Eq. [1] with increasing silica activity in the slag. An increase in temperature decreases the Gibbs energy of reaction since Eq. [1] is endothermic (see Eq. [8a]). What is evident is that Eq. [1] is spontaneous at low silica activity, down to $a_{SiO_2(s)} = 0.08$ at 1873 K (1600 °C). At the lower temperature of 1823 K (1550 °C), the reaction is not spontaneous below $a_{SiO_2(s)} = 0.28$ according to these calculations. These calculations go some way to explain the relationship between temperature and silica activity on the reactive wetting of slag, but they do not quite explain the present results where bubbling was observed in nearly all of the experiments with Slag 1, which has a silica activity of 0.15 at 1823 K (1550 °C).

### B. *Wetting and Infiltration*

Wetting in such a reactive system has been defined strictly in terms of the time-dependent "apparent"

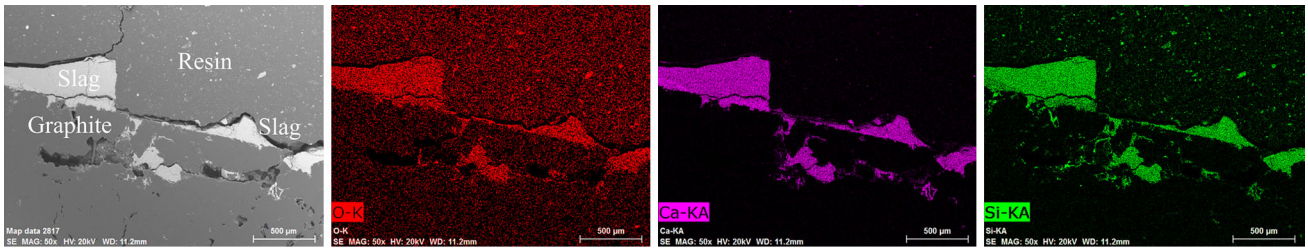


Fig. 11—SEM micrograph and EDS mapping showing extent of infiltration of Slag 1 into Graphite B at 1873 K (1600 °C) after 150 min (Run SG1). (*a*) SEM micrograph, (*b*) depth of O infiltration, (*c*) depth of Ca infiltration, and (*d*) depth of Si infiltration.

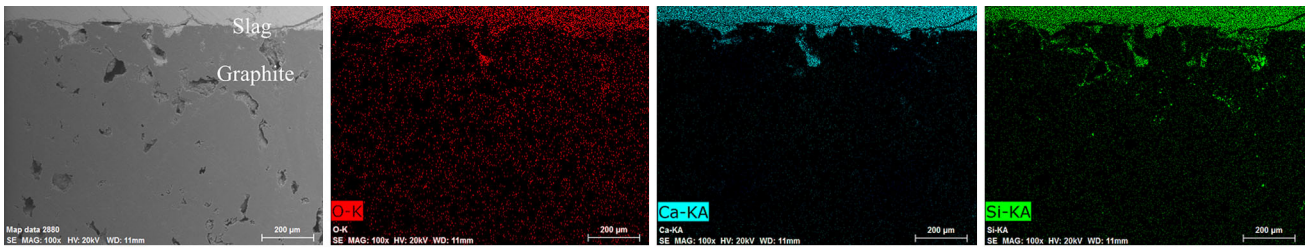


Fig. 12—SEM micrograph and EDS mapping showing extent of infiltration of Slag 1 into Graphite C at 1873 K (1600 °C) after 210 min (Run SG15). (*a*) SEM micrograph, (*b*) depth of O infiltration, (*c*) depth of Ca infiltration, and (*d*) depth of Si infiltration.

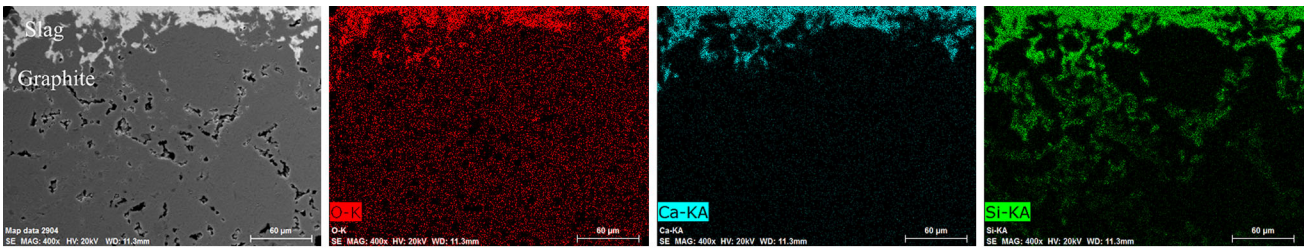


Fig. 13—SEM micrograph and EDS mapping showing extent of infiltration of Slag 2 into Graphite A at 1873 K (1600 °C) after 60 min (Run SG14). (*a*) SEM micrograph, (*b*) depth of O infiltration, (*c*) depth of Ca infiltration, and (*d*) depth of Si infiltration. Reprinted from Ref. [12].

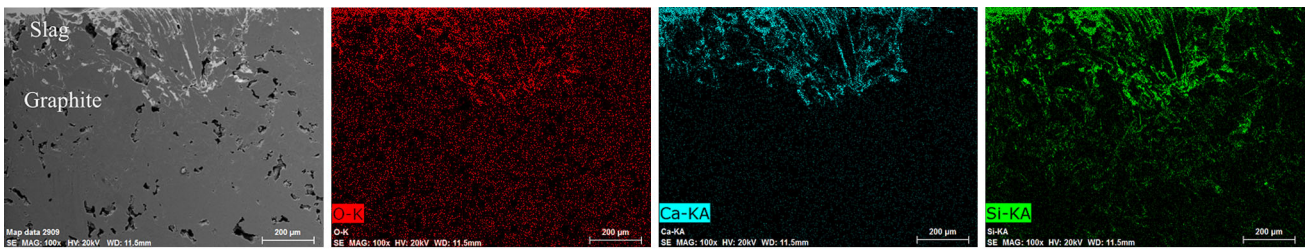


Fig. 14—SEM micrograph and EDS mapping showing extent of infiltration of Slag 2 into Graphite B at 1873 K (1600 °C) after 60 min (Run SG16). (*a*) SEM micrograph, (*b*) depth of O infiltration, (*c*) depth of Ca infiltration, and (*d*) depth of Si infiltration.

contact angle to distinguish from a static contact angle in a system at mechanical equilibrium. The total Gibbs energy is the summation of the Gibbs energy of Eq. [1] and the interfacial energy:

$$\Delta G = \Delta G_{[1]} + \gamma \cdot A \qquad [9]$$

At the onset of spreading, the reaction Gibbs energy in Eq. [9] is estimated to be many orders of magnitude

larger than the interfacial energy, as shown in Table IV. The dynamic apparent contact angle is attributed to the changing reaction Gibbs energy, $\Delta G_{[1]}$, as the interfacial reaction proceeds. Eventually, the reaction Gibbs energy attenuates as the system approaches equilibrium and the $\gamma \cdot A$ term becomes dominant. Bhoi, Ray, and Sahajwallah reached a similar conclusion in their study of FeO reduction at the slag–graphite interface.[4]

If it is the kinetics of Eq. [1] that determines the rate of spreading and infiltration, then a higher silica activity in the slag should yield a greater driving force for Eq. [1] to take place. Indeed, the rate of slag spreading is shown to increase considerably with higher silica content as seen when comparing Figures 6 through 9. Likewise, increasing the temperature should also increase the reaction rate, which leads to a faster spreading rate. This concurs with the results reported by others.[7]

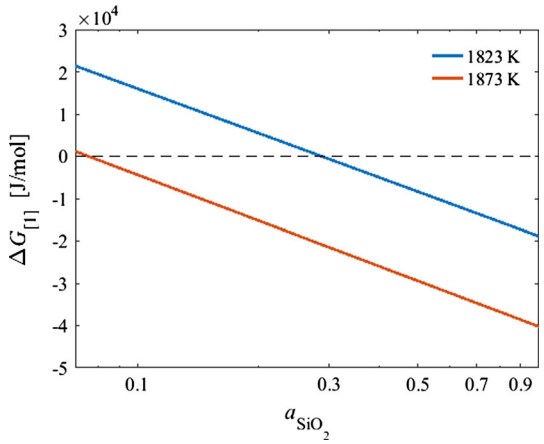


Fig. 15—Gibbs energy of Eq. [1] with increasing silica activity. Reference state is pure solid cristobalite.

**Table IV. Estimated Terms in Eq. [9] for Total Gibbs Energy**

| | |
|---|---|
| Initial slag pellet diameter (m) | 0.01 |
| Slag pellet mass (g) | 2.5 |
| Moles of $SiO_2$ in Slag 2 pellet (mol) | $2.6 \times 10^{-2}$ |
| Interfacial tension, $\gamma$ (N/m) | 0.4* |
| Interfacial area, $A$ ($m^2$) | $7.9 \times 10^{-5}$ |
| $\gamma \cdot A$ (J) | $3.9 \times 10^{-5}$ |
| $\Delta G_{[1],1873\ K\ (1600\ °C)}$, Slag 2 (J/mol) | $-3.6 \times 10^4$ |
| (J) | −936 |

*Estimation.

Liquid slag can infiltrate the open pores in the graphite substrate near the interface, the extent of which is indicated by the depth of Ca and O infiltration. The wide disparity in infiltration of the graphite grades can be attributed to open porosity, pore size and morphology, and perhaps the reactivity of the graphite. Additionally, a higher vapor pressure of SiO(g) seems to enhance silicon infiltration.

Very high ash contents in cokes have been shown to have an effect on wetting, for example, by Kang *et al.*, who studied wetting of cokes with ash contents from 11.2 to 30.3 mass pct.[8] Synthetic graphites, in contrast, have a much lower ash content. As seen in Table II, the ash contents for the graphite grades in this study are 0.03, 0.07, and 0.08 pct, for Grades A, B, and C, respectively. As such, the effect of ash content on the slag wetting of synthetic graphite is expected to be negligible.

### C. *Further Evidence for Gas–Solid Reactions*

Silicon, it appears, infiltrates much deeper into the graphite substrates than either calcium or oxygen does; this is an indication that silicon is transported into the pores of the graphite *via* the gas phase. It is hypothesized that first SiO(g) is formed as in Eq. [3], which infiltrates the open pores of the graphite substrate. Second, SiO(g) reacts with graphite on the inner surfaces of the pores to form SiC as per Eq. [4]. Figure 16 shows SEM micrographs of SiC formation in the pores from Run SG16.

### D. *Changes in Slag Composition*

Moreover, as Eq. [1] proceeds, the silica concentration in the slag should decrease; The slag composition was indeed found to change locally near the interface, as shown in Figure 17. EDS analysis and calculations show that the slag nearest the graphite interface is depleted in silica from 46 pct in the bulk slag phase down to 37.6 mass pct $SiO_2$. Inspection of Figure 2 reveals that

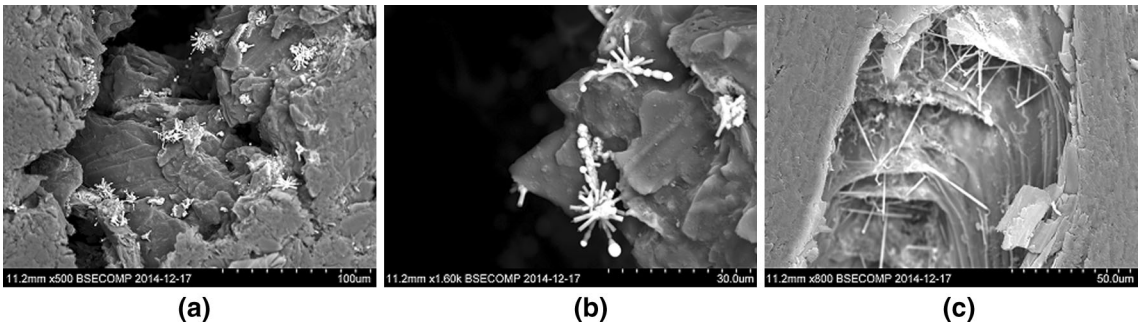


Fig. 16—SEM micrographs of SiC deposits in graphite pores from Run SG16. (*a*) Deposits of SiC in graphite pores, (*b*) deposits from (a) at higher magnification, and (*c*) Whisker growth in graphite pore.

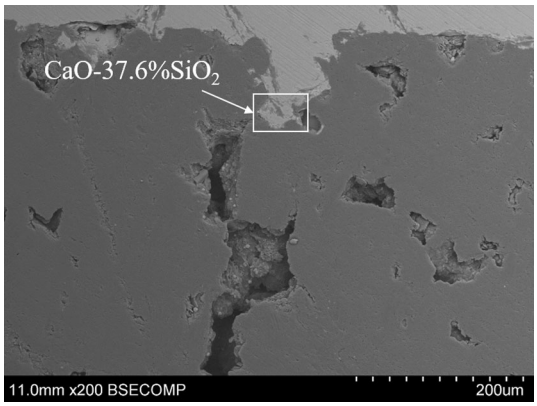


Fig. 17—Interface between Slag 1 and Graphite C from SG15 showing change in slag composition at 1873 K (1600 °C).

this composition at 1873 K (1600 °C) is in the two-phase $2CaO \times SiO_2$–liquid region.

It is plausible that depletion of $SiO_2$ in the slag phase near the interface leads to formation of a solid oxide phase at 1873 K (1600 °C), halting the reaction at the interface and infiltration by forming a diffusion barrier, effectively passivating the interface.

## V. CONCLUSIONS

Wetting of graphite by CaO-$SiO_2$ slag has been found to be quite complex. Some salient conclusions can be drawn from the current study:

1. The wetting and infiltration behavior of slag with graphite is highly material dependent. The lowest apparent contact angles are attained on Graphite B for both slag compositions. Synthetic graphites are not simple materials; the graphite recipe, grain size, open porosity, pore distribution, reactivity (available surface area), and manufacturing method all come into play.
2. The reduction of silica generates gaseous products occurred during spreading of slag on graphite as evidenced by the observation of bubble formation and silicon infiltration much deeper into the graphite substrates than the slag phase itself, indicating transport of SiO(g).
3. Increased temperature and silica activity of the slag both have a major influence on how slag spreads and infiltrates. The higher the temperature and silica content is, the greater the slag infiltration and the faster the rate of spreading. Calculations indicate that the Gibbs energy for the reduction of silica is the main driving force for spreading of slag on graphite.
4. Fundamentally, for a reactive system such as this, the driving force for spreading is the movement of the system toward a lower total Gibbs energy, in which the interfacial Eq. [1] is the dominating contribution to Eq. [9].
5. Reduction of silica in the slag near the interface may eventually lead to the formation of a solid, CaO-rich layer, slowing or stopping the reduction reaction.

An immediate industrial application of this knowledge is that "slag washing" of the graphite refractory can be an effective way of passivation to extend the lifespan of the refractory. How amenable a particular graphite is to passivation is not straightforward just judging by grain size and open porosity. For this application, good wetting is preferred, with adequate infiltration to "seal" the graphite. Less important in this application is the rate of spreading.

## ACKNOWLEDGMENTS

The authors would like to thank Elkem AS for their generous financial support.

## OPEN ACCESS



## REFERENCES

1. A.S. Mehta and V. Sahajwalla: *Scand. J. Metall.*, 2000, vol. 29, pp. 17–29.
2. N. Siddiqi, B. Bhoi, R.K. Paramguru, V. Sahajwalla, and O. Ostrovski: *Ironmaker Steelmaker*, 2000, vol. 27, pp. 367–72.
3. S.L. Teasdale and P.C. Hayes: *ISIJ Int.*, 2005, vol. 45, pp. 634–41.
4. B. Bhoi, H.S. Ray, and V. Sahajwalla: *IE(I) J-MM*, 2008, vol. 89, pp. 3–8.
5. P. Migas and M. Karbowniczek: *Arch. Metall. Mater.*, 2010, vol. 55, pp. 1147–57.
6. P. Shen, H. Fujii, and K. Nogi: *Mater. Chem. Phys.*, 2009, vol. 114, pp. 681–86.
7. V. Sahajwalla, A.S. Mehta, and R. Khanna: *Metall. Mater. Trans. B*, 2004, vol. 35B, pp. 75–83.
8. T.W. Kang, S. Gupta, S. Saha-Chaudhury, and V. Sahajwalla: *ISIJ Int.*, 2005, vol. 45, pp. 1526–35.
9. J.S. Oh and J. Lee: *J. Mater. Sci.*, 2016, vol. 51, pp. 1813–19.
10. S.-H. Heo, K. Lee, and Y. Chung: *Trans. Nonferrous Metal Soc.*, 2012, vol. 22, pp. s870–75.
11. J.F. White, L. Ma, K. Forwald, and D. Sichen: *Metall. Mater. Trans. B*, 2013, vol. 45B, pp. 150–60.
12. J.F. White, J. Lee, O. Hessling, and B. Glaser: *10th International Conference on Molten Slags, Fluxes and Salts*, May 22-25, Seattle, WA, 2016.
13. V.D. Eisenhüttenleute (ed.): *Slag Atlas*, 2nd ed., Verlag Stahleisen GmbH Düsseldorf, 1995, p. 359.
14. C.W. Bale, E. Bélisle, P. Chartrand, S.A. Decterov, G. Eriksson, K. Hack, I.H. Jung, Y.B. Kang, J. Melançon, A.D. Pelton, C. Robelin, and S. Petersen: *FactSage Thermochemical Software and Databases—Recent Developments*, Calphad, 2009, vol. 33, pp 295–311, www.factsage.com.
15. P.D. Miller, J.G. Lee, and I.B. Cutler: *J. Am. Ceram. Soc.*, 1979, vol. 62, pp. 147–49.
16. J.J. Biernacki and G.P. Wotzak: *J. Am. Ceram. Soc.*, 1989, vol. 72, pp. 122–29.
17. D.H. Flisinger and D.B. Bourrie: *J. Am. Ceram. Soc.*, 1990, vol. 73, pp. 1726–32.
18. A. Schei, J.K. Tuset, and H. Tveit: *Production of High Silicon Alloys*, Tapir Forlag, Trondheim, 1998.
19. V. Sahajwalla, C. Wu, R. Khanna, N.S. Chaudhury, and J. Spink: *ISIJ Int.*, 2003, vol. 9, pp. 1309–15.